11470 *Biochemistry* **2009,** *48,* 11470–11477
DOI: 10.1021/bi901256y

BIOCHEMISTRY
including biophysical chemistry & molecular biology
Article

ATP-Induced Conformational Changes in Hsp70: Molecular Dynamics and Experimental Validation of an in Silico Predicted Conformation[†]

Hyung-June Woo,*[,‡] Jianwen Jiang,[§] Eileen M. Lafer,[§] and Rui Sousa[§]

[‡]*Department of Chemistry, University of Nevada, Reno, Nevada 89557-0216 and* [§]*Department of Biochemistry, University of Texas Health Sciences Center, San Antonio, Texas 78229*

Received July 22, 2009; Revised Manuscript Received October 14, 2009

ABSTRACT: The 70 kDa heat shock proteins (Hsp70s) play important roles in preventing the misfolding of proteins and repairing damage under stress by coupling ATP binding and hydrolysis to protein substrate release and binding, respectively. ATP binding is believed to induce closing of the Hsp70 nucleotide binding domain (NBD) around the nucleotide. We report here a combined computational−experimental study of this open−closed transition. All-atom molecular dynamics simulations were performed for isolated open state NBDs with and without bound ATP. The nucleotide-free NBD samples a wide range of open configurations exhibiting flexible rearrangements of its four subdomains (IA-IIB). In contrast, the ATP-bound Hsp70 NBD closes to a range of configurations that is substantially more closed than the conformation observed in crystals of ATP-complexed NBDs. The close approach of subdomains IB and IIB observed in the simulations results in a strong coordination of the fluorescence probe Trp90 of IB with Arg261 of IIB, a feature not seen in the crystal structures. To determine if this computationally observed conformation occurs in solution, we constructed an R261A mutant. The mutation was found to increase the K_m and k_{cat} for ATP and to significantly reduce the extent of the fluorescence quench observed upon ATP binding. Our results thus account for the previously unexplained ATP-driven change in Trp90 fluorescence seen in the isolated NBD.

Members of the 70 kDa heat shock protein (Hsp70) family, ubiquitously found in many different species, perform a wide variety of chaperonic activities, including protecting nascent polypeptides synthesized by ribosomes from misfolding and aggregation, as well as repairing them under stress (*1*−*3*). Hsp70s are composed of a substrate binding domain (SBD)[1] that binds protein substrates and a nucleotide binding domain (NBD) that acts as an ATPase. The Hsp70 NBD (*4*) displays the hexokinase fold (*5*) with four subdomains (IA, IB, IIA, and IIB) wrapped around the nucleotide binding pocket (Figure 1). Binding of ATP is expected to induce the closing of the NBD around the nucleotide, which then induces opening of the SBD to allow protein substrate release (*4*). The presentation of a substrate to the SBD is often performed by J protein cochaperones that also stimulate ATP hydrolysis by the NBD (*6*, *7*). The ADP·NBD-SBD:substrate complex is stable, releasing the substrate slowly. A completion of the cycle therefore requires the release of ADP, which can be rate-limiting and is accelerated by the action of nucleotide exchange factors (NEFs), which include GrpE (*8*, *9*), Bag-1 (*10*), and Hsp110 (*11*, *12*).

Crystal structures of Hsp70s in complex with these NEFs reveal the NBDs in open conformations (Figure 1), and an open NBD is also observed in the nucleotide-free structure of a two-domain bovine Hsc70 (*13*). These observations suggest that opening of the NBD is required to allow nucleotide exchange to occur and that the open NBD is the favored conformation of the nucleotide-free Hsc70. However, structures of isolated Hsp70 NBDs reveal a similar closed state for the NBD, irrespective of whether ATP, ADP, or no nucleotide is bound (*4*, *7*, *14*). Thus, the latter structures provide little insight into the conformational changes induced by nucleotides and suggest that the crystal structures of the isolated NBDs are capturing a single conformational state rather than revealing the full conformational range present in solution. This would be consistent with the conclusion of Zuiderweg and co-workers, who used NMR techniques (*15*−*17*) to obtain direct evidence that the conformational flexibility of isolated Hsp70 NBDs in solution is greater than the limited range seen in the crystal structures and found that the relative orientations of Hsp70 NBD lobes I (subdomains IA and IB) and II (subdomains IIA and IIB) in solution deviate from the crystal structures by up to 10°, with sizable contributions from movements between domains IA and IIA as well as domains IA and IB.

That the crystal structures do not reveal the full range of conformational changes induced in the NBD by nucleotide binding is also suggested by experiments in which these changes are monitored by measuring fluorescence from the single Hsp70 tryptophan (Trp90 in bovine Hsc70) located in NBD subdomain IB (Figure 2). Thanks to fundamental studies pioneered by Barkley and co-workers (*18*, *19*), interpretations of fluorescence experiments on the atomic level are now becoming feasible. Experimentally, it is observed that the binding of ATP to an isolated Hsp70 NBD induces a rapid reduction (of approximately 5% at 320 nm) in the fluorescence emission from this tryptophan. With a full-length Hsp70, ATP binding induces a second slow reduction (of approximately 7−10%) in fluorescence (*20*).

[†]The work at the University of Texas was supported by the grants from the National Institutes of Health (GM052522 to R.S. and NS029051 to E.M.L.).

*To whom correspondence should be addressed. Telephone: (775) 784-1406. Fax: (775) 784-6804. E-mail: woo@unr.edu.

[1]Abbreviations: Hsc, heat shock cognate protein; Hsp, heat shock protein; SBD, substrate binding domain; NBD, nucleotide binding domain; NEF, nucleotide exchange factor; MD, molecular dynamics; PDB, Protein Data Bank; rmsd, root-mean-square deviation.

 Published on Web 11/02/2009

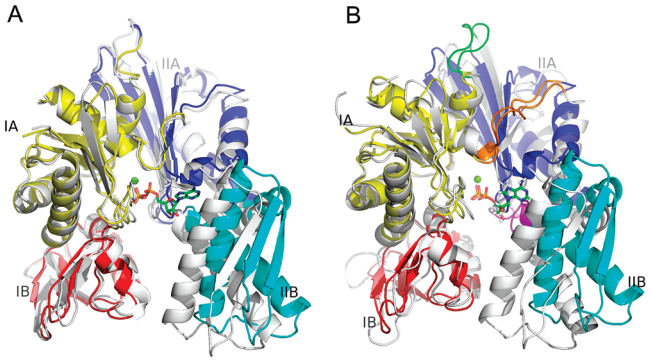

FIGURE 1: Nucleotide binding domain of bovine Hsp70. (A) Comparison of the crystallographic closed state (PDB entry 1kax, white) and open state (PDB entry 3c7n, colored), shown superimposed to minimize the rmsd of the C_α atoms of domains IB, IA, and IIA only, illustrating one mode of opening by NEF where the IIB domain rotates. (B) Comparison of the crystallographic open state, which is the initial structure of MD (PDB entry 3c7n, colored) and a late-stage snapshot (24 ns) of the ATP-bound MD trajectory (white), aligned using domains IB and IA. Both domains IIA and IIB show sizable rearrangements. The four subdomains are shown labeled as IA (yellow), IB (red), IIA (blue), and IIB (cyan). The bound ATP is shown as colored sticks, and the Mg ion is shown as a green sphere. The angle of the open−closed transition is defined as that formed by the centers of mass of domains IB, IA/IIA, and IIB. The hinge regions are shown in panel B colored as follows: orange for residues 357−366, magenta for residues 226−231, and green for residues 186−191 (see Figure 5).

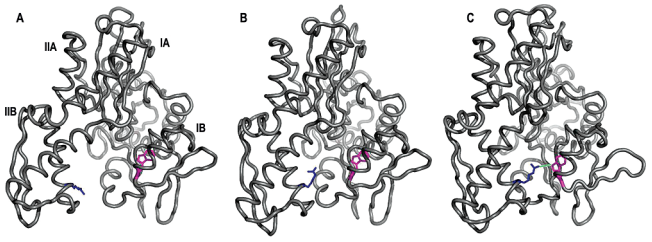

FIGURE 2: NBD closing and Trp90−Arg261 interaction. (A) Ribbon model of the open Hsp70 NBD from the Bag-1 complex [PDB entry 1hx1 (*10*)]. The Arg261 and Trp90 side chains are shown in stick representation and colored blue and magenta, respectively. (B) Ribbon model of the closed ATP-bound Hsp70 NBD [PDB entry 1kax (*14*, *30*)]. Subdomain IIB has swung toward subdomain IB, but the environment around Trp90 remains unaltered. (C) Snapshot of the "extremely closed" state of the Hsp70 NBD from the MD simulation (Supporting Information). Subdomain IIB has moved even closer toward subdomain IB, and Arg261 form a hydrogen bond with Trp90.

The latter reduction in fluorescence is coupled to the conformational change in the SBD that results in substrate release (*2*). It has thus been proposed that interactions between NBD subdomain IIB and helical elements of the SBD alter the environment around the tryptophan and account for the slow phase in the biphasic reduction in tryptophan fluorescence in full-length Hsp70 (*21*). However, the environment around Trp90 in crystal structures of open Hsp70 NBDs in nucleotide-free states (*7*, *10*, *22*−*24*) is essentially identical to that seen in isolated, closed NBDs in complexes with ATP or ADP (*14*) (Figure 2). These structures cannot, therefore, account for the rapid ATP-driven quenching of tryptophan fluorescence that is seen even in isolated NBDs.

To address the questions raised by these observations, and to provide a more complete picture of the conformational dynamics of the Hsp70 NBD in solution, we have performed molecular dynamics (MD) simulations of Hsp70 NBDs to explore the conformational changes induced by ATP binding. Numerous computational studies have been performed for similar allosteric open−closed transitions using techniques such as normal-mode analysis (*25*), all-atom MD simulations (*26*, *27*), free energy sampling (*28*), and transition path sampling (*29*). Oloo et al. (*26*), in particular, have performed all-atom simulations of the NBD of the maltose ABC transporter, a system closely related to the chaperonic NBDs, explicitly showing that ATP binding induces the closure of NBD.

Our MD simulations indicate that, unlike what is observed in crystal structures of isolated NBDs (*7*), the nucleotide-free NBD assumes an open conformation while exhibiting a large degree of flexibility in its lobe orientations. The ATP-bound NBD, on the other hand, assumes a conformation that is even more tightly closed than that seen in crystal structure of a closed ATP-bound NBD (*30*). This more complete closing is accompanied by a relative rotation of the two main lobes of the NBD, which allows coordination of the fluorescence probe Trp90 in subdomain IB by Arg261 of the approaching subdomain IIB (Figure 2 and the movie in the Supporting Information). The coordination seen in our simulations would contribute strongly to the stabilization of the tightly closed conformation observed in the ATP-bound NBD. The formation of the tightly closed state presumably leads to changes in the solvation environment of Trp90 and the quench observed in its fluorescence signal.

That this coordination may be coupled to the ATP-driven decrease in Trp90 fluorescence seen in isolated NBDs was explicitly tested by constructing and characterizing an R261A mutant. In agreement with the predictions from the MD simulations, we found that this mutation increases K_m and k_{cat} for ATP hydrolysis and nearly eliminates the ATP-driven decrease in tryptophan fluorescence in the NBD. Our studies thus provide a more complete picture of the solution dynamics of the Hsp70 chaperone and of the role of nucleotides in modulating these conformational dynamics.

MATERIALS AND METHODS

Model Building. The model open state NBD of bovine Hsp70 was built from the Hsp70−Hsp110 complex crystal structure (PDB entry 3c7n) (*22*). The isolated NBD was taken as the domain consisting of residues 1−384 by truncation of the C-terminal linker and SBD domains of the intact Hsp70. The missing residues 1 and 2 at the N-terminus were built and added to the structure. Hydrogen atoms were built using the HBUILD module of CHARMM (*31*). The protein was solvated in a pre-equilibrated water box of orthorhombic symmetry, and overlapping water molecules were deleted. K^+ and Cl^- ions were added such that the overall system is neutral and would approximate an ionic strength of 150 mM. The positions of ions were chosen randomly inside the box, avoiding direct overlap with protein atoms. The solvated system had approximately 76000 atoms. The system was energy-minimized first for 500 steps with the protein atoms fixed and then for an additional 500 steps with only crystallographic atomic positions fixed. The third energy minimization was with all atoms freed for 500 steps. The nucleotide-free model thus built did not have nucleotide inside the pocket. The ATP-bound model was built by aligning the closed crystal structure [PDB entry 1kax (*30*)] with the open state model using all four subdomains and importing the coordinates of Mg·ATP. The counterions were adjusted to make the system

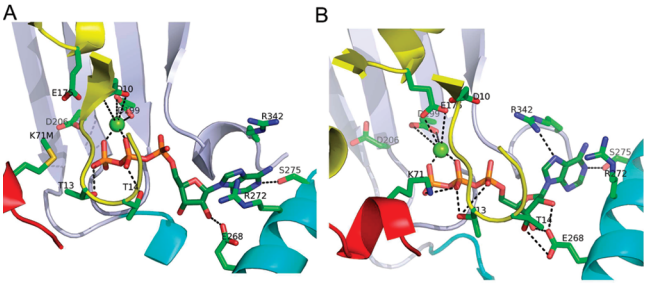

FIGURE 3: Nucleotide binding pocket configuration of the closed state Hsp70 NBD. (A) Crystal structure [PDB entry 1kax (*30*), K71M mutant]. (B) Snapshot from the ATP-bound MD trajectory at 24 ns.

neutral. Similar energy minimizations were performed for the ATP-bound open state model.

Simulation Conditions. All simulations and analysis were conducted using CHARMM version c33b2 (*31*). The CHARMM force field version 22 for protein (*32*) and version 27 for ATP (*33*, *34*) were used. The TIP3P model was used for water (*35*). The model systems were initially heated gradually to 300 K via velocity rescaling, and subsequent MD simulations were generally performed at a constant temperature of 300 K. Constant-pressure conditions were used initially to equilibrate the box size, with the production simulations largely performed in a constant volume. Constant-pressure runs were occasionally mixed in to re-equilibrate the box. Periodic boundary conditions were used with particle mesh Ewald (*36*) for electrostatic interactions and a van der Waals cutoff of 10 Å. The SHAKE algorithm was used to fix hydrogen covalent bond lengths with an integration time step of 2 fs. The protein center of mass was harmonically held at the center to avoid drifting, but otherwise, the dynamics were unconstrained. Both the nucleotide-free and ATP-bound NBD simulations were performed for more than 44 ns, which took ~12 months with parallel runs on two processors of Opteron 2214 chips per trajectory.

Analysis of Trajectories. The dynamical trajectories saved one snapshot per 0.8 ps. The subdomain rotation angle was defined as the angle formed by the centers of mass of subdomains IB, IA/IIA, and IIB. All atoms in each group were included in the calculation of the center of mass. The saved coordinates of 0.8 ps periods were used to generate the time series in Figure 4 and the statistics in Table 2. The crystal structure angles listed in Table 1 were calculated using the center of mass coordinates of atom groups of known crystal coordinates only. All root-mean-square deviation (rmsd) values were calculated with the C_α atoms of the protein backbone only. The hydrogen bond distance between Trp90 and Arg261 shown in Figure 4C was defined as the minimum distance among those between the HE1 atom of Trp90 and the NH1 or NH2 atoms of Arg261.

Preparation of Mutant and Wild-Type (WT) NBDs and Enzyme Assays. Mutants were constructed and Hsp70 NBDs expressed and purified as described previously (*7*, *13*). Single-turnover ATPase assays were conducted as described previously (*7*, *13*) and resolved by TLC. ATPase rates were determined by fitting the percent remaining [α-^{32}P]ATP at different reaction times to a single-exponential decay function using nonlinear curve fitting as implemented in Origin. V_{max} and K_m were then determined by fitting ATPase rates to enzyme concentrations using the Michaelis–Menten equation in Origin. Tryptophan fluorescence emission spectra were collected for proteins at 1 mg/mL in 10 mM Tris (pH 7.5), 50 mM KCl, and 5 mM $MgCl_2$ in either the presence or absence of 0.1 mM ATP. Data were collected on a Horiba Jovin Yvon FluoroMax 3 fluorimeter with excitation at 295 nm (1 nm bandwidth) with emission measured over the 300–380 nm window (4 nm bandwidth). Protein spectra were corrected by subtraction of emission spectra of buffer alone or buffer with 0.1 mM ATP from spectra of proteins in the absence or presence of 0.1 mM ATP, respectively.

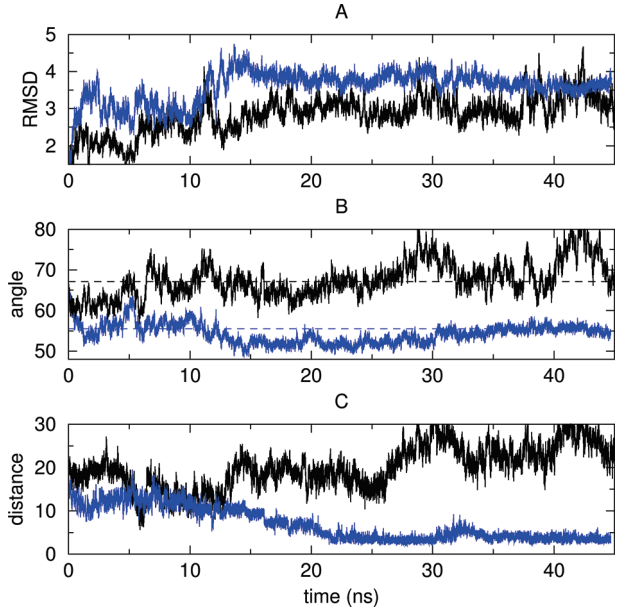

FIGURE 4: Time evolution of structural parameters over the dynamical trajectories. Black and blue lines are for the nucleotide-free and ATP-bound NBDs, respectively. (A) C_α rmsd with respect to the initial crystallographic open state (PDB entry 3c7n). (B) Domain angle between IB–(IA/IIA)–IIB centers of mass. The dashed lines indicate the angles of the crystallographic open (PDB entry 3c7n) and closed (PDB entry 1kax) states (Table 1). (C) Trp90–Arg261 hydrogen bond distance.

Table 1: Subdomain Angles of Known Closed (PDB entry 1kax) and Open Crystal Structures of the Hsp70 NBD[a]

	1kax	3c7n, Hsp110	3d2f, Hsp110	1hx1, Bag-1	3cqx, Bag-2	1yuw
crystal	55.4	67.1	72.4	64.9	60.8	62.3
MD	53.6 ± 1.9	68.6 ± 4.1				

[a]The angle values are in degrees. The second row of data shows the statistics of MD trajectories started with the 3c7n NBD structure with and without bound ATP, averaged over time excluding the initial 10 ns (see Figure 4B).

Table 2: C_α rmsd Values of MD Trajectories with Respect to the Initial Open State Reference[a]

	total	IB	IA	IIA	IIB	IB/IA	IA/IIA	IIA/IIB
ATP	3.77	2.33	1.47	1.50	1.29	1.98	2.93	1.83
nucleotide-free	3.08	2.43	1.68	1.67	1.58	2.21	2.21	2.56

[a]Snapshots along the trajectories were first aligned to the reference using the whole NBD, each subdomain, or the pairs of subdomains, and the rmsd calculated. The subdomains were defined as follows: IA, residues 1–39, 116–188, and 361–384; IB, residues 40–115; IIA, residues 189–228 and 307–360; and IIB, residues 229–306. The data shown are the root-mean-square average (in units of angstroms) over trajectories excluding the initial 10 ns (see Figure 4A).

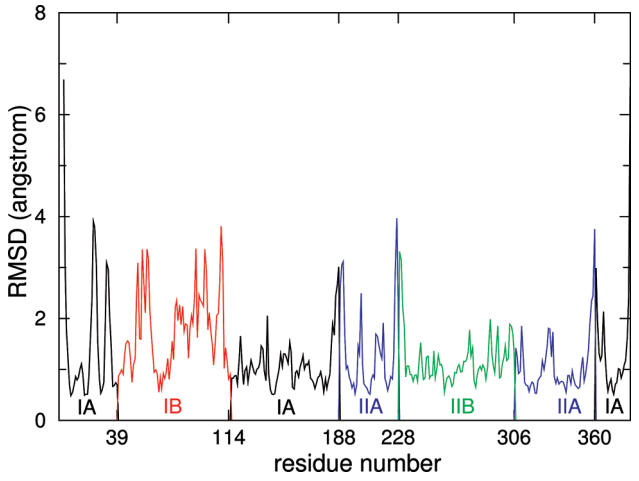

FIGURE 5: Individual contributions of residues to subdomain rmsds relative to the initial structure. For each residue, the MD snapshots were first aligned to the reference only using the subdomain to which it belongs, and the rmsd values of subdomains calculated.

RESULTS

ATP Binding Pocket Configuration. In our MD simulations, the initial state of the NBD was modeled by the open bovine Hsc70 NBD from the Hsp110-bound structure [PDB entry 3c7n (*22*)]. From this state, two trajectories were initiated: one with a bound ATP and the other nucleotide-free. We generated the initial structure of the ATP-bound NBD was generated by aligning the open NBD from the Hsp110−Hsc70 complex with the structure of a more closed NBD with bound ATP (PDB entry 1kax) and then importing the Mg·ATP coordinates. If in carrying out this alignment one optimizes superposition of lobe I from each NBD, then the ATP is docked so that the interactions with the phosphate groups are favorably formed. Alternatively, if the alignment optimizes superposition of lobe II, then the interactions with the base are retained. Instead, we chose to minimize bias toward interactions with either the base or phosphates in our initial model of the ATP-bound open NBD by optimizing a global alignment that involved all four subdomains of the NBDs. In addition to the Mg^{2+} ion, two K^+ ions near the ATP in the binding pocket play roles in the hydrolytically active closed state of the NBD (*37*). These potassium ions were not included in our initial ATP-bound open model, although ions (K^+ and Cl^-) were present around the protein within the solvent region. Our dynamical simulation is therefore intended to probe the early-stage collapse of the NBD, induced by a relatively unspecific Mg·ATP binding event.

After 24 ns (Figure 3B), many of the interactions of key residues with Mg·ATP in the binding pocket are observed to form. Some differences with the crystal structure, however, are seen, notably with Thr13, which is mainly coordinated to β-P_i rather than γ-P_i. Thr13 plays a key role in the transmission of the ATP-induced conformational change to the SBD (*38*). To see if a manual placement of potassium ions would quickly establish some of the remaining nucleotide−protein interactions, a late-stage snapshot was taken from the dynamical trajectory, and two potassium ions nearby were physically moved to the putative locations suggested by the crystal structure. A subsequent dynamics run, however, did not reveal any rapid changes in the binding modes of key residues.

Closing of the Cleft in the ATP-Bound NBD. We quantify the large-scale structural transition between the open and closed states with the domain angle formed by the centers of mass of subdomains IB, IA/IIA, and IIB (Figure 1). Table 1 compares the angle values of some of the known NEF-bound NBD crystal structures, the nucleotide-free two-domain structure, and the closed state value (PDB entry 1kax, 55.4°). The open NBDs can be grouped into two classes: in the Bag-1 (*10*) and Hsp110 (*22*, *23*) complexes, rearrangement into the open state is largely confined to the rotation of subdomain IIB (Figure 1A) and involves the IIA−IIB interface. In the complex with Bag-2 (*24*) and in the two-domain nucleotide-free Hsp70 (*13*), the conformational change also includes the relative rotation of lobes I and II with respect to each other and involves the IA−IIA interface. The difference in the opening angles between the two Hsp70−Hsp110 complexes is likely due to differences in the nucleotides bound in each complex: due to differences in the crystal growth conditions, PDB entry 3c7n has a bound ADP in the Hsc70 NBD while PDB entry 3d2f, which is ~5° more open, does not. The former therefore probably represents an intermediate in the ADP release process driven by Hsp110. Overall, the data in Table 1 suggest that the action of NEF binding generally forces the NBD to open more than the nucleotide-free form without NEF, with varying degrees of domain opening reflecting both the nature of the bound NEF and nucleotides captured within the pocket in the crystals.

Our simulation results provide dynamical information about the NBD opening modes and flexibility, which complement the structural data. Figure 4A shows the evolution of the rmsd of the NBD relative to the initial open state. Both the nucleotide-free and ATP-bound NBDs exhibit equilibration within ~15 ns, during which the ATP-bound NBD accumulates relatively larger deviations from the reference. The larger magnitude of the rmsd (by ~0.7 Å) of the ATP-bound NBD compared to the nucleotide-free NBD reflects the subdomain closing from the open state.

This closing is more clearly seen in Figure 4B, which shows the time series of the subdomain angle along the two trajectories. It is notable that for both nucleotide-free and ATP-bound NBDs, the early subnanosecond trends exhibit a precipitous drop in angle from the initial value corresponding to the Hsp110 complex. This behavior implies that irrespective of the nucleotide inside the pocket, the conformation of the NBD within the complex is stabilized by the bound NEF. Without the NEF in our simulations, the particular open state adopted by the NBD becomes unstable, leading to a quick initial collapse of the domain angle both for the nucleotide-free NBD and for the ATP-bound NBD. This temporary closing of the nucleotide-free NBD, however, is gradually offset by a reopening of the subdomains in ~10 ns. The average of the angle for nucleotide-free NBD after this period agrees well with what would be expected on the basis of the values of crystal structures (Table 1). Our nucleotide-free trajectory nevertheless implies that the open form adopted by the NBD in NEF complexes differs considerably from the native open form most stable for an isolated NBD.

The domain angle of the ATP-bound NBD in contrast exhibits an equilibration into values that are ~15° smaller than the open average. This range of values is more closed (by ~2°) than the crystal structure of an ATP-bound NBD. The degree of fluctuation around the average (1.9°) is also much smaller than for the nucleotide-free NBD (4.0°), suggesting that intrinsic flexibility in subdomain movements in the nucleotide-free form is suppressed in the closed NBD by interactions with ATP.

Contribution of Subdomain Movements. The subdomain movements constituting the open−closed transition largely

consist of rigid body-type hinge bending motions of the four subdomains, IB, IA, IIA, and IIB (Figure 1). To quantify this feature, the overall rmsd of the whole NBD (Figure 4A) was compared with those calculated using individual or collections of subdomains (Table 2), and the contribution that each domain movement makes to the large-scale conformational change was assessed. For both nucleotide-free and ATP-bound NBDs, it is seen that subdomain IB shows the largest internal conformational change and flexibility. As can be seen in Figure 1B, such internal changes in IB largely consist of partial unfolding of the β-sheet secondary structure in the simulated NBDs. The rest of the subdomains all exhibit relatively small internal rmsd values ($\sim$1.4 Å), revealing the rigidity of the subdomain folds.

To examine the roles played by the hinge bending rearrangements of subdomains in the closing transition, we bundled adjacent subdomains into pairs and calculated the rmsd values of these groups with respect to the open state reference (Table 2). For the ATP-bound NBD, the IB/IA pair shows an rmsd value (2.0 Å) that is intermediate between those for the individual subdomains. Domain pairs IA/IIA and (to a lesser extent) IIA/IIB, in contrast, both show rmsds much larger than the individual subdomain values. This suggests that the greatest contribution (2.9 Å) to the closing transition in the ATP-bound NBD comes from hinge motions in the interface between the IA and IIA subdomains, or relative rotations of lobes I and II (Figure 1). This largest change is followed by the movements (1.8 Å) in the interface between subdomains IIA and IIB. The rmsd of the IB/IA pair (2.0 Å), in contrast, is mainly a consequence of the internal flexibility of the IB subdomain (intradomain rmsd of 2.3 Å).

The rmsd values of the nucleotide-free NBD, on the other hand, largely reflect the flexibility of subdomain movements around the open state: the values of the three interdomain pairs are all similar in magnitude (2.2, 2.2, and 2.6 Å). We therefore conclude that in the open form, all four subdomains undergo relatively large rigid body-type rearrangements.

More information about the distribution of subdomain flexibility within the NBD can be gleaned from the contribution each residue makes to the conformational changes. Figure 5 shows such a distribution for the ATP-bound NBD trajectory. In this analysis, for each residue of the NBD, structures on the trajectory were first aligned to the initial open state using only the subdomain to which the residue belongs, and the rmsd of the chosen residue was calculated. This procedure largely removes contributions that the rigid body hinge bending movements make to the overall conformational change. The rmsd values calculated therefore mostly reflect the deviations of each residue within the subdomain, allowing for the identification of hinge regions. Apart from the flexible N- and C-terminal residues, we identify three hinge regions from Figure 5: residues 186−191 and 357−366, which form the loops at the interface between the IA and IIA subdomains, and residues 226−231 at the interface between subdomains IIA and IIB (Figure 1B). The existence of two hinges between domains IA and IIA compared to one between domains IIA and IIB also correlates well with the fact that the former makes greater contributions to the overall closing transition than the latter. Although many residues in the IB subdomain show similar levels of movement, the distribution is spread over the subdomain rather than localized, which we attribute to the internal unfolding of secondary structures.

Identification of disordered loops and hinge regions can also be achieved by bioinformatics methods, which have the advantage of speed often without the knowledge of crystal structures. Predictions for disordered regions in the Hsp70 NBD by two knowledge-based methods, FoldUnfold (*39*, *40*) and RONN (*41*), included the region of residues 226−231, which is seen to have the greatest disorder in Figure 5.

Fluorescence Probe Trp90. The nucleotide-free and ATP-bound NBD trajectories were analyzed to examine changes to the solvation environment of Trp90 located in subdomain IB. A prominent structural change expected to affect the Trp90 fluorescence signal is the coordination of the tryptophan residue by Arg261 in subdomain IIB within the ATP-bound NBD trajectory (Figures 2 and 4C). In the crystallographic open and closed structures (Figures 2A,B), the closed state flips the Arg261 side chain toward IB (from the direction facing the NEF in the open state), while the Trp90 side chain remains largely unchanged. The distance between these residues (NE1 of Trp90 and NH1/NH2 of Arg261) decreases from 21 Å in the open state (PDB entry 3c7n) to 11 Å in the closed state (PDB entry 1kax) but is always too far to allow coordination. In the simulation of the nucleotide-free NBD, the Trp90−Arg261 distance fluctuates between 14 and 30 Å, again reflecting fluctuating subdomain rearrangements (Figure 4C). The distance in the ATP-bound NBD, in contrast, steadily decreases over $\sim$20 ns from 21 to 3.8 $\pm$ 0.9 Å (> 22 ns). These late-stage values correspond to conformations in which the two residues steadily maintain hydrogen bonds (Figure 2C and the movie in the Supporting Information). It was also observed that together with Trp90, the neighboring His89 interacts with Arg261.

Mutational Test of Predictions from the MD Simulation of ATP-Induced Closing of Hsp70. Our MD simulation suggests that ATP binding induces a more extreme closing of the NBD than what has been observed crystallographically, resulting in extensive contacts between subdomains IB and IIB and formation of a hydrogen bond between Arg261 and Trp90 of the Hsp70 NBD (Figure 2C). Such a conformational change would alter the environment of the tryptophan and could be responsible for the ATP-driven reduction in tryptophan fluorescence seen in the isolated NBD. To test this, we characterized an Hsp70 NBD in which Arg261 had been substituted with alanine. The available crystal structures suggest that such a mutation should have no effect on ATP hydrolysis, affinity, or ATP-induced changes in tryptophan fluorescence since this arginine makes no direct interactions with ATP or the tryptophan and is not involved in stabilizing the closed NBD conformation in these structures.

However, the MD results predict that (1) an R261A mutation will increase ATP K_m by removing an interaction that stabilizes the extremely closed NBD, thus facilitating ATP dissociation [as has been observed previously for mutations in residues that are far from the ATP binding site but that stabilize the closed conformation through interactions between NBD subdomains IB and IIB (*42*)], and (2) an R261A mutation will reduce or abrogate the ATP-induced change in tryptophan fluorescence.

Single-turnover ATPase assays revealed that the R261A mutation increases the K_m for ATP by $\sim$5-fold, consistent with the prediction from the MD simulation (Figure 6A,B). The mutation also increases the ATPase rate by $\sim$6-fold. Such increases in ATPase rates have been seen in many Hsp70 mutants (*7*, *13*, *43*, *44*), including mutants in residues that are distant from the active site, and may reflect the fact that the ATP·Hsp70 complex is conformationally restricted in a state with a low ATPase rate that is dynamically activated through

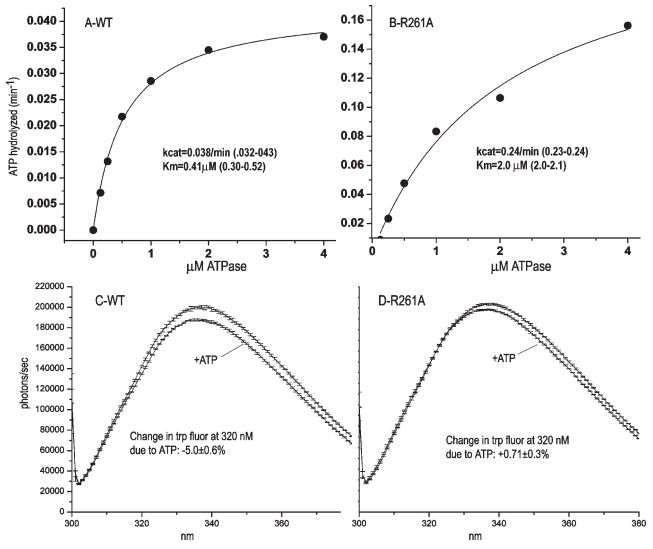

FIGURE 6: ATP hydrolysis rates as a function of WT (A) or R261A (B) NBD concentrations in single-turnover ATPase reactions. Fits are to the Michaelis−Menten equation, and presented values give averages and the range (in parentheses) from two independent determinations. Tryptophan fluorescence emission spectra for WT (C) or R261A (D) NBDs in the absence or presence of 0.1 mM ATP (as indicated). Error bars spanning the spectra show the standard deviation for four independent experiments, as are the presented values for the effects of ATP on the spectra at 320 nm.

interactions with J-proteins or mutations that increase the mobility of this state.

Addition of ATP to the WT NBD resulted in a 5% decrease in tryptophan fluorescence at 320 nm (the decrease at 339 nm was 7%), in agreement with previous measurements (*20*, *45*) (Figure 6C). The R261A mutant, however, exhibited a barely detectable 0.7% increase in tryptophan fluorescence at 320 nm and an only 3% decrease at 339 nm (Figure 6D). These results support the conclusion from the MD simulation that, in solution, ATP induces a greater closure of the NBD than is seen in the crystal structures, so that subdomain IB moves close enough to IIB to allow Arg261 to form a hydrogen bond to Trp90 and cause a change in the environment of this tryptophan that can explain the ATP-induced change in fluorescence seen in the isolated NBD.

DISCUSSION

Studies using tryptophan fluorescence (*20*) have revealed the sequence of conformational changes induced by binding of ATP to bovine Hsc70: the first step is a bimolecular reaction of ATP and NBD accompanied by a rapid fluorescence intensity quench; the second step is a much slower ($k \simeq 0.7\ s^{-1}$) isomerization corresponding to a conformational change involving both the NBD and the SBD. With the (44 kDa) NBD fragment, only the initial, rapid bimolecular step is observed. However, crystal structures of isolated NBDs provide no insight into these changes since the environment around the tryptophan (and the degree of opening of the NBD) is essentially identical in these structures irrespective of the nucleotide state of the NBD. This suggests that the conformational range of the NBD in solution is more extensive than that observed in the crystal structures, a conclusion that is supported by NMR studies (*15*−*17*). Our MD simulations identify the structural change that is likely to be responsible for the ATP-driven fluorescence change in the isolated NBD: subdomain IIB's approach to IB results in a strong coordination of Trp90 by Arg261 (Figure 4C). The fast time scale (~20 ns) of this change in the simulation is consistent with the single-step bimolecular nature of the experimentally observed fluorescence quench. The fact that a relatively unspecific placement of a Mg·ATP in the pocket (without the catalytic potassium ions) was sufficient to cause the rapid collapse of the NBD suggests that NBD closure is largely driven by a collective electrostatic interaction that does not require precise participation of catalytic residues. The close approach of subdomains IB and IIB, in particular, is made possible both by the more complete closing of the two lobes compared to the crystal structures and by a sizable rotation of lobe II with respect to lobe I (Figures 1 and 2). The latter feature is consistent with previously observed structural features of the nucleotide-free two-domain Hsp70 structure (*13*), the Bag-2 NEF complex structure (*24*), and the Hsbp1 NEF complex (*46*).

We note that studies of isolated tryptophans in solution have established that their fluorescence signals are not quenched appreciably by arginines alone (*18*, *19*). The observed coordination of Trp90 by Arg261, therefore, is likely to be causing the quench by stabilizing the tightly closed ATP-bound conformation and altering the solvation environment of Trp90 with its neighboring residues, rather than quenching the fluorescence directly with the hydrogen bond. This interpretation is reinforced by the observation of the "flipping" of the Trp90 side chain in the movie in the Supporting Information, apparently driven by its interaction with Arg261.

Our simulations also reveal that a nucleotide-free NBD samples a broad range of open conformations with fluctuations that support the picture of the Hsp70 NBD as a four-subdomain protein joined by flexible interfaces, consistent with models based on NMR experiments (*15*). The greater flexibility of the nucleotide-free versus nucleotide-bound NBD is also supported by the observation of much higher thermal factors for crystal structures of otherwise identical nucleotide-free (PDB entry 2qw9) versus ADP-bound (PDB entry 2qwl) or ADP·Vi-bound NBDs (PDB entry 2qwm) (*13*). It is worth noting that the nucleotide-free crystal structure (PDB entry 2qw9) is closed despite the absence of bound nucleotides. Given the flexibility of the nucleotide-free NBD indicated by Figure 4B, it is reasonable to interpret this as a consequence of packing contacts in crystals of isolated NBDs.

The initial collapse observed in these simulations commences within a surprisingly short time scale (~10 ns) accessible with direct all-atom MD, with the ATP placed in the middle of the open binding site. Completion of specific interactions of key residues with ATP to the level seen in crystal structures (Figure 3), however, would likely require time scales considerably longer than 44 ns sampled in this study. One may thus envision a scenario for the open−closed transition akin to those in protein folding processes, where the dynamical processes are divided into two main stages. In the first stage, the insertion of a nucleotide ligand causes a relatively unspecific collapse of subdomains toward the binding pocket. Diffusional drifts of the NBD would then follow within the restricted conformational space in which the subdomains have already "closed" but key interactions still have not been completed (analogous to the molten globule phase in protein folding). This second stage of drifts would be terminated by a "lock-in" event when the full set of key interactions become established and would involve time scales that are orders of magnitude longer.

These latter steps would likely be coupled to the global conformational changes of the intact Hsp70 that involve both

the NBD and the SBD (*21*). Computational investigations of these slower steps will require different strategies, focused on efficient samplings of conformational spaces and nucleotide−protein residue interactions. An important conclusion from our studies, nevertheless, is that MD simulations can reveal enough details regarding novel conformational states to allow explicit testing (and validation) by biochemical approaches.

SUPPORTING INFORMATION AVAILABLE

Coordinate file for the closed state NBD from a late-stage snapshot (24 ns) of the ATP-bound trajectory (Figure 2C) and a movie illustrating the closing of the ATP-bound NBD (blue lines in Figure 4) from the initial open state (cartoons in gray color), where the viewpoint corresponds to the direction from the bottom to top in Figure 1. The frame rates are 0.1 ns/frame for the first 24 and 0.4 ns/frame for 24−44 ns. This material is available free of charge via the Internet at http://pubs.acs.org.

REFERENCES

1. Bukau, B., Deuerling, E., Pfund, C., and Craig, E. A. (2000) Getting newly synthesized proteins into shape. *Cell 101*, 119–122.
2. Mayer, M. P., Brehmer, D., Gassler, C. S., and Bukau, B. (2002) Hsp70 chaperone machines. *Adv. Protein Chem. 59*, 1–44.
3. Mayer, M. P., and Bukau, B. (2005) Hsp70 chaperons: Cellular functions and molecular mechanism. *Cell. Mol. Life Sci. 62*, 670–684.
4. Flaherty, K. M., Deluca-Flaherty, C., and McKay, D. B. (1990) 3-dimensional structure of the ATPase fragment of a 70K heat-shock cognate protein. *Nature 346*, 623–628.
5. Bennett, W. S., and Steitz, T. A. (1980) Structure of a complex between yeast hexokinase-A and glucose: 2. Detailed comparisons of conformation and active-site configuration with the native hexokinase-B monomer and dimer. *J. Mol. Biol. 140*, 211–230.
6. Walsh, P., Bursac, D., Law, Y. C., Cyr, D., and Lithgrow, T. (2004) The J-protein family: Modulating protein assembly, disassembly, and translocation. *EMBO Rep. 5*, 567–571.
7. Jiang, J., Maes, E. G., Taylor, A. B., Wang, L., Hinck, A. P., Lafer, E. M., and Sousa, R. (2007) Structural basis of J cochaperone binding and regulation of Hsp70. *Mol. Cell 28*, 422–433.
8. Packschies, L., Theyssen, H., Buchberger, A., Bukau, B., Goody, R. S., and Reinstein, J. (1997) GrpE accelerates nucleotide exchange of the molecular chaperone DnaK with an associative displacement mechanism. *Biochemistry 36*, 3417–3422.
9. Harrison, C. J., Hayer-Hartl, M., Di Liberto, M., Hartl, F.-U., and Kuriyan, J. (1997) Crystal structure of the nucleotide exchange factor GrpE bound to the ATPase domain of the molecular chaperone DnaK. *Science 276*, 431–435.
10. Sondermann, H., Scheufler, C., Schneider, C., Hohfeld, J., Hartl, F. U., and Moarefi, I. (2001) Structure of a Bag/Hsc70 complex: Convergent functional evolution of Hsp70 nucleotide exchange factors. *Science 291*, 1553–1557.
11. Dragovic, Z., Broadley, S. A., Shomura, Y., Bracher, A., and Hartl, F. U. (2006) Molecular chaperones of the Hsp110 family act as nucleotide exchange factors of Hsp70s. *EMBO J. 25*, 2519–2528.
12. Raviol, H., Sadlish, H., Rodriguez, F., Mayer, M. P., and Bukau, B. (2006) Chaperone network in the yeast cytosol: Hsp110 is revealed as an Hsp70 nucleotide exchange factor. *EMBO J. 25*, 2510–2518.
13. Jiang, J., Prasad, K., Lafer, E. M., and Sousa, R. (2005) Structural basis of interdomain communication in the Hsc70 chaperone. *Mol. Cell 20*, 513–524.
14. Flaherty, K. M., Wilbanks, S. M., DeLuca-Flaherty, C., and McKay, D. B. (1994) Structural basis of the 70-kilodalton heat shock cognate protein ATP hydrolytic activity: II. Structure of the active site with ADP or ATP bound to wild type and mutant ATPase fragment. *J. Biol. Chem. 269*, 12899–12907.
15. Zhang, Y. B., and Zuiderweg, E. R. P. (2004) The 70-kDa heat shock protein chaperone nucleotide-binding domain in solution unveiled as a molecular machine that can reorient its functional subdomains. *Proc. Natl. Acad. Sci. U.S.A. 101*, 10272–10277.
16. Revington, M., Holder, T. M., and Zuiderweg, E. R. P. (2004) NMR study of nucleotide-induced changes in the nuclear binding domain of *Thermus thermophilus* Hsp70 chaperone DnaK: Implications for the allosteric mechanism. *J. Biol. Chem. 279*, 33958–33967.
17. Revington, M., Zhang, Y., Yip, G. N. B., Kurochkin, A. V., and Zuiderweg, E. R. P. (2005) NMR investigations of allosteric processes in a two-domain *Thermus thermophilus* Hsp70 molecular chaperones. *J. Mol. Biol. 349*, 163–183.
18. Chen, Y., and Barkley, M. D. (1998) Toward understanding tryptophan fluorescence in proteins. *Biochemistry 37*, 9976–9982.
19. Adams, P. D., Chen, Y., Ma, K., Zagorski, M. G., Sönnichsen, F. D., McLaughlin, M. L., and Barkley, M. D. (2002) Intramolecular quenching of tryptophan fluorescence by the peptide bond in cyclic hexapeptides. *J. Am. Chem. Soc. 124*, 9278–9286.
20. Ha, J.-H., and McKay, D. B. (1995) Kinetics of nucleotide-induced changes in the tryptophan fluorescence of the molecular chaperone Hsc70 and its subfragments suggest the ATP-induced conformational change follows initial ATP binding. *Biochemistry 34*, 11635–11644.
21. Liu, Q., and Hendrickson, W. A. (2007) Insights into Hsp70 chaperone activity from a crystal structure of the yeast Hsp110 Sse1. *Cell 131*, 106–120.
22. Schuermann, J. P., Jiang, J., Cuellar, J., Llorca, O., Wang, L., Gimenez, L. E., Jin, S., Taylor, A. B., Demeler, B., Morano, K. A., Hart, P. J., Valpuesta, J. M., Lafer, E. M., and Sousa, R. (2008) Structure of the Hsp110:Hsc70 nucleotide exchange macine. *Mol. Cell 31*, 232–243.
23. Polier, S., Dragovic, Z., Hartl, F. U., and Bracher, A. (2008) Structural basis for the cooperation of Hsp70 and Hsp110 chaperones in protein folding. *Cell 133*, 1068–1079.
24. Xu, Z., Page, R. C., Gomes, M. M., Kohli, E., Nix, J. C., Herr, A. B., Patterson, C., and Misra, S. (2008) Structural basis of nucleotide exchange and client binding by the Hsp70 cochaperone Bag2. *Nat. Struct. Mol. Biol. 15*, 1309–1317.
25. Brooks, B., and Karplus, M. (1985) Normal modes for specific motions of macromolecules: Application to the hinge-bending mode of lysozyme. *Proc. Natl. Acad. Sci. U.S.A. 82*, 4995–4999.
26. Oloo, E. O., Fung, E. Y., and Tieleman, D. P. (2006) The dynamics of the MgATP-driven closure of MalK, the energy-transducing subunit of the maltose ABC transporter. *J. Biol. Chem. 281*, 28397–28407.
27. Colombo, G., Morra, G., Meli, M., and Verkhivker, G. (2008) Understanding ligand-based modulation of the Hsp90 molecular chaperone dynamics at atomic resolution. *Proc. Natl. Acad. Sci. U.S.A. 105*, 7976–7981.
28. Faraldo-Gómez, J. D., and Roux, B. (2007) On the importance of a funneled energy landscape for the assembly and regulation of multidomain Src tyrosine kinases. *Proc. Natl. Acad. Sci. U.S.A. 104*, 13643–13648.
29. Radhakrishnan, R., and Schlick, T. (2004) Orchestration of cooperative events in DNA synthesis and repair mechanism unraveled by transition path sampling of DNA polymerase β's closing. *Proc. Natl. Acad. Sci. U.S.A. 101*, 5970–5975.
30. O'Brien, M. C., Flaherty, K. M., and McKay, D. B. (1996) Lysine 71 of the chaperone protein Hsc70 is essential for ATP hydrolysis. *J. Biol. Chem. 271*, 15874–15878.
31. Brooks, B. R., Bruccoleri, R. E., Olafson, B. D., States, D. J., Swaminathan, S., and Karplus, M. (1983) CHARMM: A program for macromolecular energy, minimization, and dynamics calculations. *J. Comput. Chem. 4*, 187–217.
32. MacKerell, A. D., Jr., Bashford, D., Bellott, M., Dunbrack, R. L., Jr., Evanseck, J. D., Field, M. J., Fischer, S., Gao, J., Guo, H., Ha, S., Joseph-McCarthy, D., Kuchnir, L., Kuczera, K., Lau, F. T. K., Mattos, C., Michnick, S., Ngo, T., Nguyen, D. T., Prodhom, B., Reiher, W. E.III, Roux, B., Schlenkrich, W., Smith, J. C., Stote, R., Straub, J., Watanabe, M., Wiorkiewicz-Kuczera, J., Yin, D., and Karplus, M. (1998) All-atom empirical potential for molecular modeling and dynamics studies of proteins. *J. Phys. Chem. B 102*, 3586–3616.
33. Foloppe, N., and MacKerell, A. D., Jr. (2000) All-atom empirical force field for nucleic acids: I. Parameter optimization based on small molecule and condensed phase macromolecular target data. *J. Comput. Chem. 32*, 86–104.
34. MacKerell, A. D., Jr., and Banavali, N. K. (2000) All-atom empirical force field for nucleic acids: II. Application to molecular dynamics simulations of DNA and RNA in solution. *J. Comput. Chem. 21*, 105–120.
35. Jorgensen, W. L., Chandrasekhar, J., Madura, J. D., Impey, R. W., and Klein, M. L. (1983) Comparison of simple potential functions for simulating liquid water. *J. Chem. Phys. 79*, 926–935.
36. Essman, U., Perera, L., Berkowitz, M. L., Darden, T., Lee, H., and Pedersen, L. G. (1995) A smooth particle mesh Ewald method. *J. Chem. Phys. 103*, 8577–8593.
37. Wilbanks, S. M., and McKay, D. B. (1995) How potassium affects the activity of the molecular chaperone Hsc70: II. Potassium

binds specifically in the ATPase active-site. *J. Biol. Chem. 270*, 2251–2257.
38. Sousa, M. C., and McKay, D. B. (1998) The hydroxyl of threonine 13 of the bovine 70-kDa heat shock cognate protein is essential for transducing the ATP-induced conformational change. *Biochemistry 37*, 15392–15399.
39. Galzitskaya, O. V., Garbuzynskiy, S. O., and Lobanov, M. Y. (2006) FoldUnfold: Web server for the prediction of disordered regions in protein chain. *Bioinformatics 22*, 2948–2949.
40. Galzitskaya, O. V., Garbuzynskiy, S. O., and Lobanov, M. Y. (2006) Prediction of amyloidogenic and disordered regions in protein chains. *PLoS Comput. Biol. 2*, 1639–1648.
41. Yang, Z. R., Thomson, R., McNeil, P., and Esnouf, R. M. (2005) RONN: The bio-basis function neural network technique applied to the detection of natively disordered regions in proteins. *Bioinformatics 21*, 3369–3376.
42. Brehmer, D., Rudiger, S., Gassler, C. S., Klostermeier, D., Packchies, L., Reinstein, J., Mayer, M. P., and Bukau, B. (2001) Tuning of chaperone activity of Hsp70 proteins by modulation of nucleotide exchange. *Nat. Struct. Biol. 8*, 427–432.
43. Vogel, M., Bukau, B., and Mayer, M. P. (2006) Allosteric regulation of Hsp70 chaperones by a proline switch. *Mol. Cell 21*, 359–367.
44. Laufen, T., Mayer, M. P., Beisel, C., Klostermeier, D., Mogk, A., Reinstein, J., and Bukau, B. (1999) Mechanism of regulation of Hsp70 chaperones by DnaJ cochaperones. *Proc. Natl. Acad. Sci. U.S.A. 96*, 5452–5457.
45. Johnson, E. R., and McKay, D. B. (1999) Mapping the role of active site residues for transducing an ATP-induced conformational change in the bovine 70-kDa heat shock cognate protein. *Biochemistry 38*, 10823–10830.
46. Shomura, Y., Dragovic, Z., Chang, H.-C., Tzvetkov, N., Young, J. C., Brodsky, J. L., Guerriero, V., Hartl, F. U., and Bracher, A. (2005) Regulation of Hsp70 function by HspBP1: Structural analysis reveals an alternate mechanism for Hsp70 nucleotide exchange. *Mol. Cell 17*, 367–379.